Turkish Journal of Electrical Engineering & Computer Sciences

http://journals.tubitak.gov.tr/elektrik/

Research Article

Turk J Elec Eng & Comp Sci
(2019) 27: 1157 – 1171

doi:10.3906/elk-1806-214

A generalized switching function-based discontinuous space vector modulation technique for unbalanced two-phase three-leg inverters

Watcharin SRIRATTANAWICHAIKUL*
Department of Electrical Engineering, Faculty of Engineering, Chiang Mai University, Chiang Mai, Thailand

Received: 29.06.2018 • **Accepted/Published Online:** 17.12.2018 • **Final Version:** 22.03.2019

Abstract: This paper presents a discontinuous space vector modulation technique for unbalanced two-phase three-leg inverters. This technique is based on the shift-angle and generalized modulation algorithm obtained for generating the unbalanced two-phase output voltage. Furthermore, the discontinuous switching sequence intends to improve the commutations of power switching devices in each inverter leg that achieves a minimum number of switching state changes in one sampling cycle. Therefore, the switch commutations can be reduced by one-third in one main period. The step-by-step procedure of the modulation algorithm for easy implementation in a digital control platform is discussed. The performance of the developed modulation technique is verified through both simulation and experimental results in a nonunity power factor balanced two-phase load and asymmetrical two-phase induction motor drive.

Key words: Two-phase system, three-leg inverter, DC/AC conversion, space vector modulation

1. Introduction

In order to confront the reduced switching losses and high-performance requirements for inverters, low switching frequency operations and modified modulation techniques have intensively been studied [1–5]. The discontinuous space vector modulation (SVM) techniques are more widely used for better performance of the inverter, in which each phase of the inverter is clamped to either negative or positive DC-link voltage for an interval of one-third in one main period. It can reduce the switching losses compared with the continuous SVM or carrier-based pulse-width modulation (CBPWM) [6–12].

The standard three-leg inverter can generate balanced and unbalanced two output voltages. It has been extensively applied to two-phase load systems such as the adjustable-speed drive of the two-phase induction motors [13–17], the single-phase three-wire inverter for battery energy storage systems [18], and single-phase three-wire photovoltaic energy conversion systems [19, 20]. In recent years, the research topics of the modulation technique for the balanced and unbalanced two output voltages using the three-leg inverter topology mainly include the reduction of output current ripple, reduction of switching frequency, modification of the modulation algorithm, and low switching frequency operation [17, 21].

Several efforts have been proposed in the literature for improving the performance of the two-phase three-leg inverter based on SVM techniques. The SVM technique was first used for the two-phase three-leg inverter in order to control the two-phase induction motor drive [14]. This paper focused on the continuous SVM technique for generating the balanced two output voltages. The output current waveform is less distorted because the

*Correspondence: watcharin.s@eng.cmu.ac.th

low-order harmonics are not present in the output voltage. The expressions of the continuous SVM technique for the unbalanced two-phase three-leg inverter were presented in [16] and the switching losses and current ripple reduction based on discontinuous SVM technique were introduced in [17]. This technique can reduce the output current ripple and switching losses at high modulation index operation. However, the switching sequence selection has not been discussed. Moreover, the limitation of this technique is that the location of the active voltage vectors divides into ten sectors, which complicates the switching sequences.

The main contribution of this paper is the proposal of the discontinuous SVM technique for an unbalanced two-phase three-leg inverter that will ensure a minimum number of switching state changes in one sampling cycle in order to reduce the commutation of the power switching devices in each leg of the inverter. A generalized method for the SVM algorithm can be applied to any two-phase three-leg inverter. The paper is organized as follows. Section 2 describes the two-phase system of the three-leg inverter. The proposed discontinuous SVM algorithm to control unbalanced two output voltages is discussed in Section 3. The simulation and experimental results, which verify the modulation technique, are discussed in Section 4. The output current and voltage waveforms and total harmonic-distorted output voltages are presented and discussed. Finally, the conclusion is given in Section 5.

2. Two-phase three-leg inverter system configuration

Currently, the balanced and unbalanced two-phase voltage can be developed using the standard three-phase inverter. This inverter topology has been widely used in industry for the adjustable-speed drives of two-phase induction machines. The typical power stage of a three-leg inverter for a two-phase load system is shown in Figure 1. There is a full-bridge converter having six power switches, with an antiparallel free-wheeling diode with each. The constant DC-link voltage by rectifier is delivered to the input inverter. Generally, the two output voltages can be controlled independently using the three-leg inverter with a modulation technique.

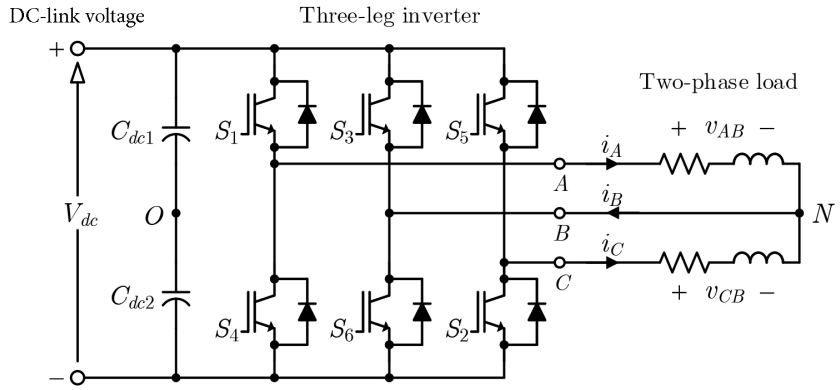

Figure 1. Simplified circuit diagram of the two-phase three-leg inverter.

Based on the equivalent circuit in Figure 1, the output pole voltages in each leg of the inverter are given by

$$v_{AO} = \frac{m_a V_{dc}}{2} \cos\left(\omega_s t - \frac{\pi}{2}\right), \quad (1)$$

$$v_{BO} = \frac{m_a V_{dc}}{2} \cos\left(\omega_s t \pm \theta_v\right), \quad (2)$$

$$v_{CO} = \frac{m_a V_{dc}}{2} \cos\left(\omega_s t + \frac{\pi}{2}\right), \quad (3)$$

where v_{AO}, v_{BO}, v_{CO} are the pole voltages, m_a is the modulation index ($0 < m_a \leq 1.0$), V_{dc} is the DC-link voltage, $\omega_s t$ is the electrical angular, and θ_v is the shift-angle for the unbalanced two output voltages.

Considering that the three-leg inverter supplies the two-phase load, the unbalanced two output voltages v_{AB} and v_{CB} can be expressed as

$$v_{AB} = v_{AO} - v_{BO} = m_a V_{dc} \cos\left(\frac{\pi}{4} - \frac{\theta_v}{2}\right) \cos\left(\omega_s t + \frac{3\pi}{4} - \frac{\theta_v}{2}\right), \tag{4}$$

$$v_{CB} = v_{CO} - v_{BO} = m_a V_{dc} \sin\left(\frac{\pi}{4} - \frac{\theta_v}{2}\right) \cos\left(\omega_s t + \frac{3\pi}{4} - \frac{\theta_v}{2}\right), \tag{5}$$

where v_{AB} is the output voltage between leg-A and leg-B and v_{CB} is the output voltage between leg-C and leg-B.

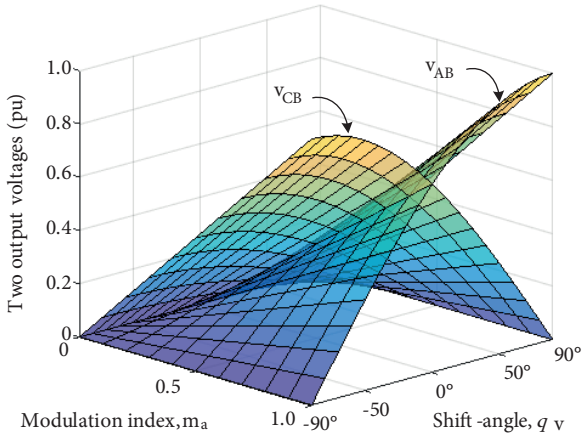

Figure 2. Surface simulated waveform of the two output voltages v_{AB} and v_{CB} in the per unit (pu) comparison with different shift-angles θ_v and modulation index m_a.

From Eqs. (4) and (5), it can be found that the unbalanced two output voltages v_{AB} and v_{CB} are obtained from the voltage difference between each voltage leg, depending on the control of the common pole voltage in leg-B. Therefore, the unbalanced two output voltages can be adjusted by the shift-angle θ_v of the common pole voltage v_{BO}. As a consequence, the two output voltages are unequal such that v_{AB} can be adjusted higher or lower than each output voltage, v_{CB}, while the phase difference of the two output voltages is kept perpendicular.

For the unbalanced output voltages, the relationship between the ratio of output voltage inverter V_{AB}/V_{CB} and shift-angle θ_v can be expressed as [21]:

$$\theta_v = 2\tan^{-1}\left(\frac{V_{AB}}{V_{CB}}\right) - \frac{\pi}{2}. \tag{6}$$

To explain the merits of the unbalanced two-phase three-leg inverter, the relationship between the shift-angle θ_v and modulation index m_a of the corresponding two output voltages in pu is shown in Figure 2. Provided that the shift-angle is a positive value ($0° < \theta_v < +90°$), v_{AB} is higher than v_{CB}, whereas for a

negative value of the shift-angle $(-90^\circ < \theta_v < 0^\circ)$, it is lower than v_{CB}. Moreover, the modulation index m_a and DC-link voltage V_{dc} are also impacted for two output voltages.

3. Proposed discontinuous SVM technique for the unbalanced two-phase three-leg inverter

Space vector modulation has the ability of fast realization in real-time applications and is widely used for digital control of inverters. The average switching frequency of the output signals can be limited in order to reduce excessive switching losses in the inverter. This section presents the discontinuous SVM technique for generating unbalanced output voltages by using the two-phase three-leg inverter.

3.1. Space vectors

The two-phase three-leg inverter can be represented by the space vector diagram. Eight voltage space vectors exist in a three-leg inverter, as shown in Figure 3. $\vec{V}_1$–$\vec{V}_6$ are active vectors, and $\vec{V}_0$ and $\vec{V}_7$ are zero vectors, which depend on the on-state of the power switches. On this plane, the six active vectors form an elliptical plane and divide into six sectors (I–VI). The zero vectors are located in the center of the elliptical plane.

Under the unbalanced space vector plane, sectors I and IV always take a 90° electrical degree while space vector planes in sectors II, III, V, and VI depend on the magnitude of the shift-angle θ_v. It can be adjusted to positive or negative directions. This means that the shift-angle θ_v influences the length of two active vectors in each sector. The elliptical space vector plane can be represented by positive and negative shift-angle directions as shown in Figures 3a and Figure 3b, respectively. The switching states of the unbalanced two-phase three-leg inverter are shown in Table 1. When the upper switch of an inverter leg is turned to "1" and the lower switch is turned off, "0", the pole voltages producing the positive DC-link voltage through the pole voltages are zero when the lower switch is turned on. Therefore, the possible eight combinations of the power switches generate the unbalanced output voltages.

3.2. Generalization of the discontinuous SVM algorithm

Figure 4 shows a block diagram of the proposed SVM algorithm with the six steps. The SVM involves several design steps and complex modeling, thus incurring a higher computational burden than the conventional modulation technique. The step-by-step procedure for designing the SVM algorithm for the unbalanced two-phase three-leg inverter is presented as follows.

Step 1: The input variables are the modulating signal m_a, the fundamental frequency f_1, and the shift-angle θ_v, which are converted into the three-phase instantaneous signals $v^*_{AO}, v^*_{BO}, v^*_{CO}$ by using the output pole voltages calculation given in Eqs. (1)–(3).

Step 2: The three-phase instantaneous modulating signals $v^*_{AO}, v^*_{BO}, v^*_{CO}$ are converted into two-phase stationary frame modulating signals v^*_{AB}, v^*_{CB} by using

$$\begin{bmatrix} v^*_{AB} \\ v^*_{CB} \end{bmatrix} = \frac{1}{\sqrt{2}} \begin{bmatrix} 1 & -1 & 0 \\ 0 & -1 & 1 \end{bmatrix} \begin{bmatrix} v^*_{AO} \\ v^*_{BO} \\ v^*_{CO} \end{bmatrix}, \tag{7}$$

where the coefficient $\frac{1}{\sqrt{2}}$ shows that the amplitude of the reference voltage will be equal to the three voltage legs after the transformation.

The reference voltage vector $\vec{v}^*_{ref}$ in the two-phase stationary frame is represented as

$$\vec{v}^*_{ref} = v^*_{AB} + jv^*_{CB}. \tag{8}$$

Table 1. Space vectors, switching states, and on-state switches of the two-phase three-leg inverter.

Space vector	Switching state	On-state switch	Vector definition
$\vec{V}_0$	[000]	S_1, S_3, S_5	0
$\vec{V}_7$	[111]	S_4, S_6, S_2	0
$\vec{V}_1$	[100]	S_1, S_6, S_2	$\vec{V}_1 = V_{dc}e^{j0}$
$\vec{V}_2$	[110]	S_1, S_3, S_2	$\vec{V}_2 = V_{dc}e^{j\frac{\pi}{2}}$
$\vec{V}_3$	[010]	S_4, S_3, S_2	$\vec{V}_3 = V_{dc}e^{j\left(\frac{3\pi}{4}\pm\theta_v\right)}$
$\vec{V}_4$	[011]	S_4, S_3, S_5	$\vec{V}_4 = V_{dc}e^{j\pi}$
$\vec{V}_5$	[001]	S_4, S_6, S_5	$\vec{V}_5 = V_{dc}e^{j\frac{3\pi}{2}}$
$\vec{V}_6$	[101]	S_1, S_6, S_5	$\vec{V}_6 = V_{dc}e^{j\left(\frac{7\pi}{4}\pm\theta_v\right)}$

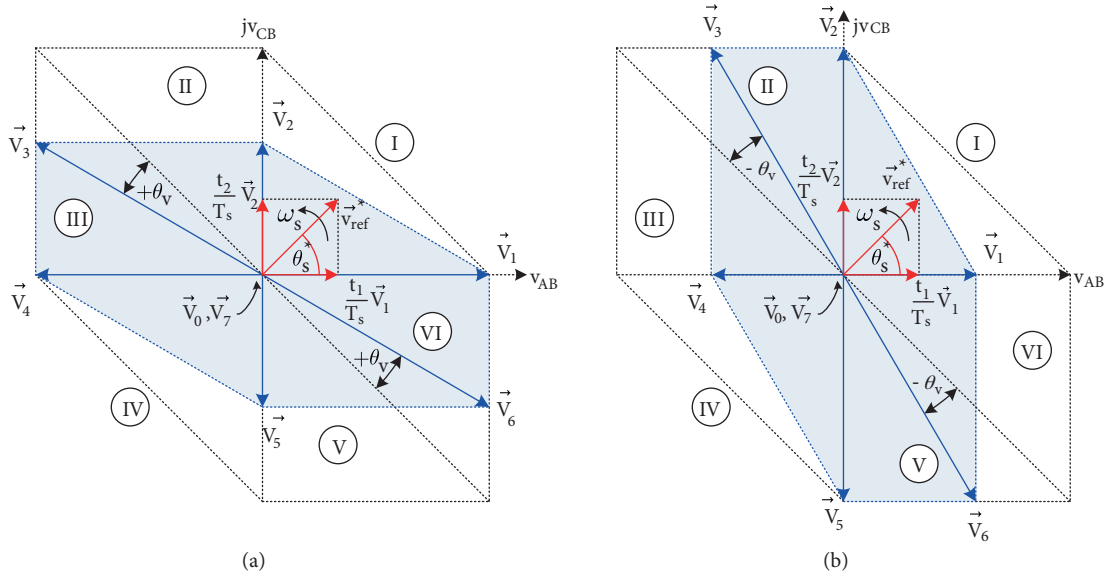

Figure 3. Operating principle of unbalanced space vector diagram for a two-phase three-leg inverter: a) the positive shift-angle condition, b) the negative shift-angle condition.

Step 3: The modulating signals in the two-phase stationary frame are transformed into the polar coordinates. Therefore, the magnitude of the reference vector $\left|\vec{v}^*_{ref}\right|$ and the angular displacement θ^*_s can be obtained by:

$$\vec{v}^*_{ref} = \left|\vec{v}^*_{ref}\right| e^{j\theta^*_s}, \quad \left|\vec{v}^*_{ref}\right| = \sqrt{v^{*2}_{AB} + v^{*2}_{CB}}, \quad \theta^*_s = \tan^{-1}\left(\frac{v^*_{CB}}{v^*_{AB}}\right). \tag{9}$$

From Eq. (9), the sector number (I–VI) is computed according to the value of angular displacement θ_s. For example, the sector number is I when θ^*_s varies between zero and $\pi/2$.

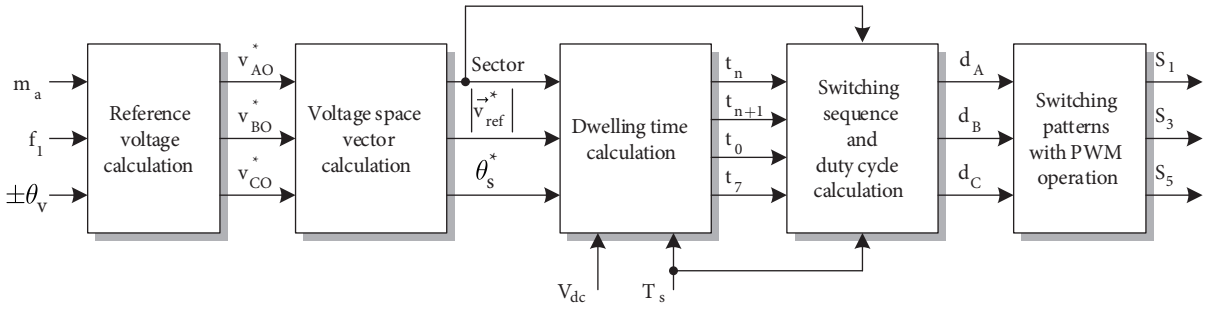

Figure 4. Block diagram of the proposed SVM algorithm.

Step 4: As shown in Figure 3, the reference voltage vector $\vec{v}^*_{ref}$ is synthesized by three nearby stationary vectors based on the gating signals generated for the inverter. Dwell times define the time duration, which are generating a voltage with the average value equal to the reference voltage vector using the summation of three voltage vectors nearest to the voltage references during a sampling time period T_s. Assuming that the reference voltage vector $\vec{v}^*_{ref}$ is constant, its amplitude in sampling time period T_s and the shift-angle θ_v are positive or negative directions. The time duration for two active vectors and one zero vector in each sector can be calculated to determine the switching states according to the following equations in Table 2.

By using sector number I as an example in Figure 3, the reference voltage vector falls in this sector. It can be synthesized to the four adjacent voltage vectors, the two basic active vectors of $\vec{V}_1$ and $\vec{V}_2$, and the zero vectors $\vec{V}_0$ and $\vec{V}_7$, with time duration t_1, t_2, t_0, and t_7 as

$$\vec{v}^*_{ref} T_s = \vec{V}_1 t + \vec{V}_2 t_2 + \vec{V}_0 \frac{t_0}{2} + \vec{V}_7 \frac{t_7}{2}, \tag{10}$$

$$T_s = t_1 + t_2 + t_0 + t_7. \tag{11}$$

To calculate the time duration in each sector as shown in Table 2, the switching time intervals of voltage vector equations in each sector can be determined by switching states.

Table 2. Dwelling time calculation.

Sector I: $\left[0 \le \theta^*_s < \frac{\pi}{2}\right]$	**Sector II:** $\left[\frac{\pi}{2} \le \theta^*_s < \left(\frac{3\pi}{4} \pm \theta_v\right)\right]$	**Sector III:** $\left[\left(\frac{3\pi}{4} \pm \theta_v\right) \le \theta^*_s < \pi\right]$
$t_1 = \frac{v^*_{ref}}{V_{dc}} T_s \cos(\theta^*_s)$	$t_3 = \frac{v^*_{ref}}{V_{dc}} T_s \frac{\cos(\theta^*_s)}{[\cos(\theta_v)+\sin(\theta_v)]}$	$t_3 = \frac{v^*_{ref}}{V_{dc}} T_s \frac{\sin(\theta^*_s)}{[\cos(\theta_v)+\sin(\theta_v)]}$
$t_2 = \frac{v^*_{ref}}{V_{dc}} T_s \sin(\theta^*_s)$	$t_2 = \frac{v^*_{ref}}{V_{dc}} T_s [\cos(\theta^*_s) + \sin(\theta^*_s)]$	$t_4 = -\frac{v^*_{ref}}{V_{dc}} T_s [\cos(\theta^*_s) + \sin(\theta^*_s)]$
$t_0 + t_7 = T_s - t_1 - t_2$	$t_0 + t_7 = T_s - t_2 - t_3$	$t_0 + t_7 = T_s - t_3 - t_4$
Sector IV: $\left[\pi \le \theta^*_s < \frac{3\pi}{2}\right]$	**Sector V:** $\left[\frac{3\pi}{2} \le \theta^*_s < \left(\frac{7\pi}{4} \pm \theta_v\right)\right]$	**Sector VI:** $\left[\left(\frac{7\pi}{4} \pm \theta_v\right) \le \theta^*_s < 2\pi\right]$
$t_5 = -\frac{v^*_{ref}}{V_{dc}} T_s \sin(\theta^*_s)$	$t_5 = -\frac{v^*_{ref}}{V_{dc}} T_s [\cos(\theta^*_s) + \sin(\theta^*_s)]$	$t_1 = \frac{v^*_{ref}}{V_{dc}} T_s [\cos(\theta^*_s) + \sin(\theta^*_s)]$
$t_4 = -\frac{v^*_{ref}}{V_{dc}} T_s \cos(\theta^*_s)$	$t_6 = \frac{v^*_{ref}}{V_{dc}} T_s \frac{\cos(\theta^*_s)}{[\cos(\theta_v)+\sin(\theta_v)]}$	$t_6 = -\frac{v^*_{ref}}{V_{dc}} T_s \frac{\sin(\theta^*_s)}{[\cos(\theta_v)+\sin(\theta_v)]}$
$t_0 + t_7 = T_s - t_4 - t_5$	$t_0 + t_7 = T_s - t_5 - t_6$	$t_0 + t_7 = T_s - t_1 - t_6$

Step 5: To improve the performance of the SVM algorithm, the discontinuous switching sequence of the unbalanced two-phase three-leg inverter also needs concentration. Figure 5 shows the switching sequences for the reference vectors dwelling in all six sectors under the positive shift-angle (Figure 5a) and negative shift-angle

(Figure 5b) conditions. It can be noted that switching sequences of the proposed algorithm can be generated the two variations, DSVM-1 and DSVM-2.

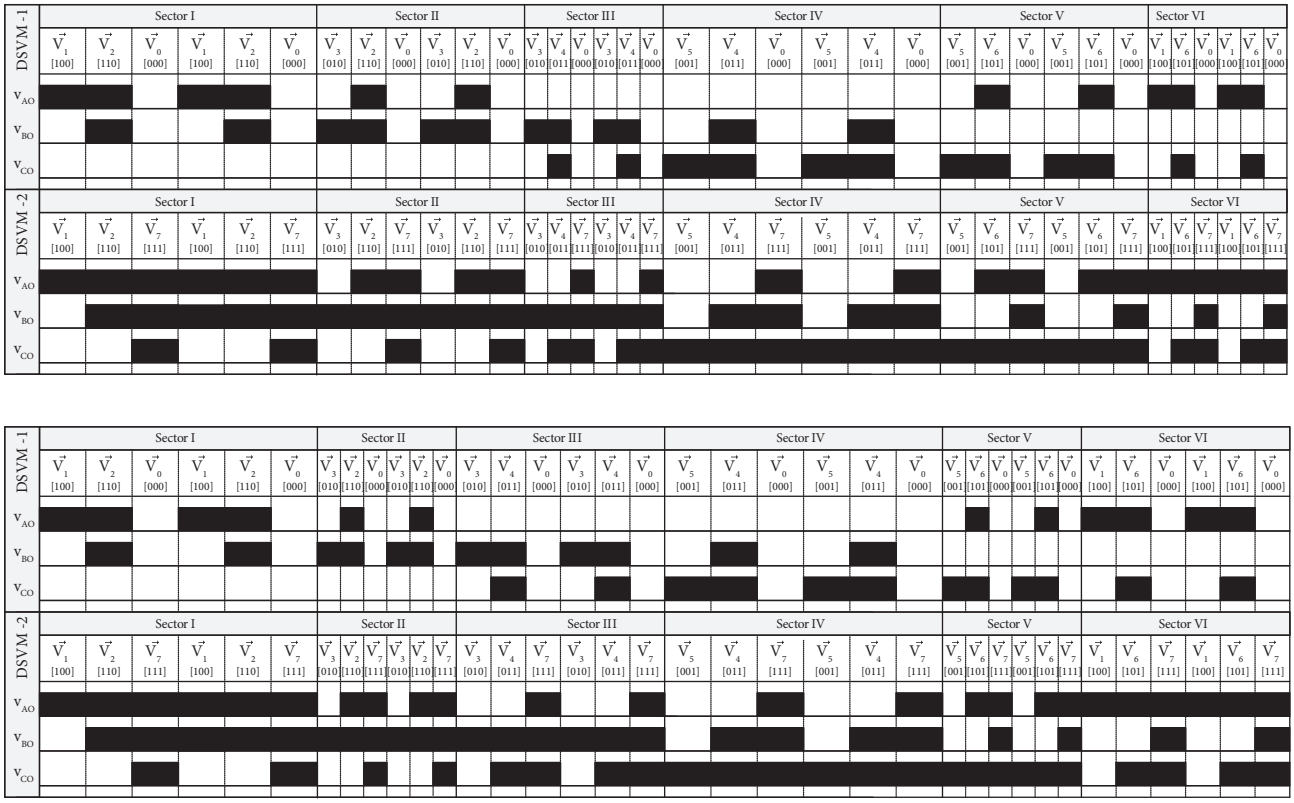

Figure 5. Switching sequences in the proposed discontinuous SVM technique for the unbalanced two-phase three-leg inverter: a) the positive shift-angle condition, b) the negative shift-angle condition.

DSVM-1 always uses $\vec{V}_0$ with a straightforward sequence. In this case, each pole voltage does not switch for one-third of its time period. It can be seen that the output pole voltages are clamped low. Similarly, DSVM-2 is involved using $\vec{V}_7$, for which the output pole voltages are clamped high. The clamped voltages mean no switching for one-third of the time period. Therefore, the proposed SVM algorithm also achieves lower switching losses.

Step 6: The corresponding duty cycles in a complete period obtained using the proposed SVM technique are given in Table 3 for DSVM-1 and Table 4 for DSVM-2. These equations are generalized and applicable to any unbalanced two-phase three-leg inverter.

4. Results and discussion

4.1. Simulation results of the discontinuous SVM technique for the nonunity power factor balanced two-phase load

This subsection presents the simulation results that the unbalanced two-phase three-leg inverter obtains using the discontinuous SVM technique. The simulation results using MATLAB/Simulink are presented to verify the proposed modulation technique. The detailed system parameters are given as follows: the nominal DC-link voltage V_{dc} is 500 V, the fundamental frequency f_1 is 50 Hz, the switching frequency f_s is 5 kHz, and the

Table 3. Duty cycle calculation in DSVM-1.

Sector I	**Sector II**	**Sector III**
$d_A = \frac{1}{T_s}(t_1 + t_2)$ $d_B = \frac{1}{T_s}(t_2)$ $d_C = 0$	$d_A = \frac{1}{T_s}(t_2)$ $d_B = \frac{1}{T_s}(t_2 + t_3)$ $d_C = 0$	$d_A = 0$ $d_B = \frac{1}{T_s}(t_3 + t_4)$ $d_C = \frac{1}{T_s}(t_4)$
Sector IV	**Sector V**	**Sector VI**
$d_A = 0$ $d_B = \frac{1}{T_s}(t_4)$ $d_C = \frac{1}{T_s}(t_4 + t_5)$	$d_A = \frac{1}{T_s}(t_6)$ $d_B = 0$ $d_C = \frac{1}{T_s}(t_5 + t_6)$	$d_A = \frac{1}{T_s}(t_1 + t_6)$ $d_B = 0$ $d_C = \frac{1}{T_s}(t_6)$

Table 4. Duty cycle calculation in DSVM-2.

Sector I	**Sector II**	**Sector III**
$d_A = \frac{1}{T_s}(t_1 + t_2)$ $d_B = \frac{1}{T_s}(t_2)$ $d_C = 1$	$d_A = \frac{1}{T_s}(t_2)$ $d_B = \frac{1}{T_s}(t_2 + t_3)$ $d_C = 1$	$d_A = 1$ $d_B = \frac{1}{T_s}(t_3 + t_4)$ $d_C = \frac{1}{T_s}(t_4)$
Sector IV	**Sector V**	**Sector VI**
$d_A = 1$ $d_B = \frac{1}{T_s}(t_4)$ $d_C = \frac{1}{T_s}(t_4 + t_5)$	$d_A = \frac{1}{T_s}(t_6)$ $d_B = 1$ $d_C = \frac{1}{T_s}(t_5 + t_6)$	$d_A = \frac{1}{T_s}(t_1 + t_6)$ $d_B = 1$ $d_C = \frac{1}{T_s}(t_6)$

modulation index m_a is constant at 1.0. The shift-angle θ_v is set at $\pm 36.87°$. The system is connected to the nonunity power factor balanced two-phase load with a 1.2 kVA, 230 V, 50 Hz, 0.9 lagging power factor.

Figure 6 shows the simulated waveform of the sector (Figure 6a), timing for active and zero vectors (Figure 6b), duty cycles (Figure 6c), and switching signals in switching sequence variations for the discontinuous SVM technique (Figure 6d). In the simulated conditions, as the switching sequences and shift-angle of the unbalanced output voltages change, the shape of modulation changes. During the span of the switching sequence and shift-angle, the shape of the duty cycles and switching signals follow the following modulations: 1) DSVM-1 for $\theta_v = +36.87°$ at $t = 0$ to 0.08 s, and 2) DSVM-2 for $\theta_v = -36.87°$ at $t = 0.08$ to 0.14 s. It can be noted that the modulation technique unifies the existing discontinuous modulations, depending on the switching sequence selections. From the waveform presented in Figure 6c and Figure 6d, it is obvious that the given is clamped either to the positive and negative states without any switching corresponding to one-third ($120°$) during the one main period of the fundamental frequency.

The simulated waveforms of the unbalanced output voltages and currents and the harmonic spectrum of voltages are given in Figure 7 and Figure 8, respectively, for the two types of discontinuous SVM switching sequences. In Figure 7a, at $\theta_v = +36.87°$ for DSVM-1, the rms values of fundamental component output voltages v_{AB} and v_{CB} are about 316.1 V and 158 V, respectively. Different switching sequences using DSVM-2 are shown in Figure 7b, where the shift-angle θ_v is a unit step change to $-36.87°$ at $t = 0.08$ s. The rms values of fundamental component output voltages v_{AB} and v_{CB} are 158.1 V and 316.3 V, respectively. It can be seen that the output voltage v_{CB} is twice higher than v_{AB}. In Figure 7c, the output currents with nonunity factor two-phase loads (i_A, i_B, and i_C) are unequal due to the unbalanced output voltages. Moreover, it can be

observed that the neutral current i_B only has to carry the summation of current between the two-phase load back to the middle leg of the inverter.

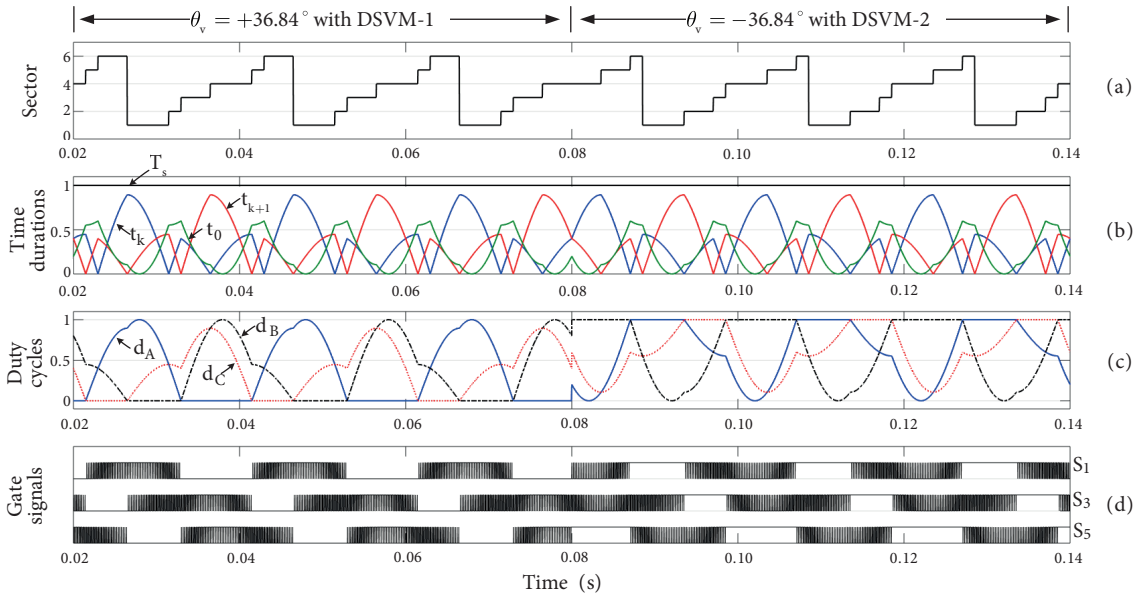

Figure 6. Simulated waveforms of the proposed discontinuous SVM technique for the unbalanced two-phase three-leg inverter: a) sector, b) time durations (k = number of sector), c) duty cycles, d) switching patterns.

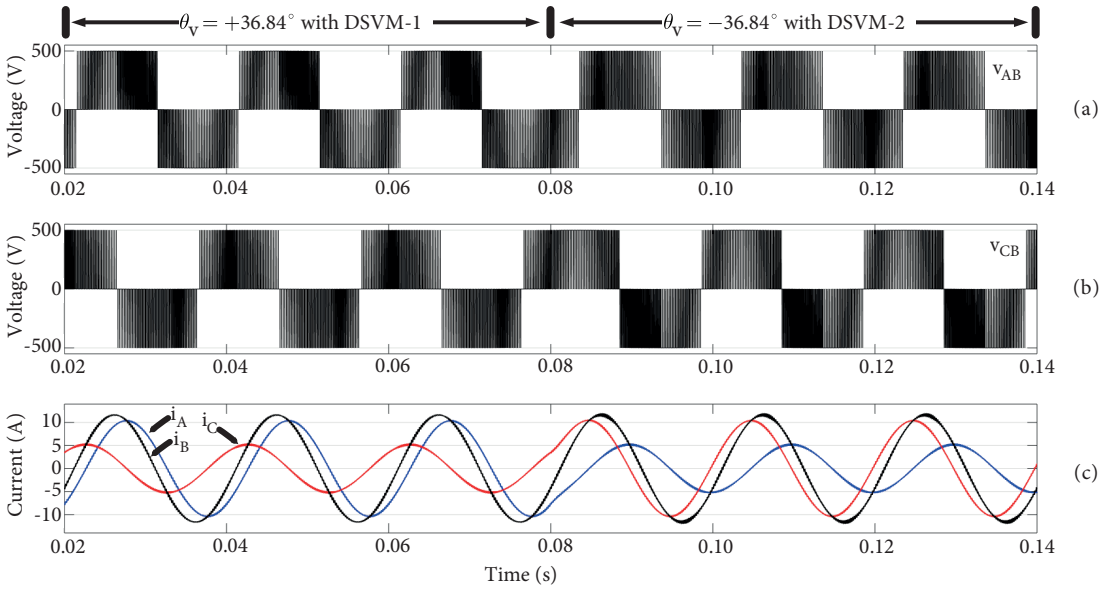

Figure 7. Simulated waveforms of the unbalanced two-phase three-leg inverter: a) output voltage v_{AB}, b) output voltage v_{CB}, c) output currents i_A, i_B, i_C.

Figure 8a and Figure 8b show the total harmonics distortion (THD) of output voltages in DSVM-1 and DSVM-2 when the shift-angle condition is changed. It is observed that the amplitude and THD of two-phase output voltages in these two cases are similar. For DSVM-2, the shift-angle is changed to a negative value as

shown in Figure 8b. It shows that the amplitude and THD of two-phase output voltages are opposite values, which is comparable to DSVM-1.

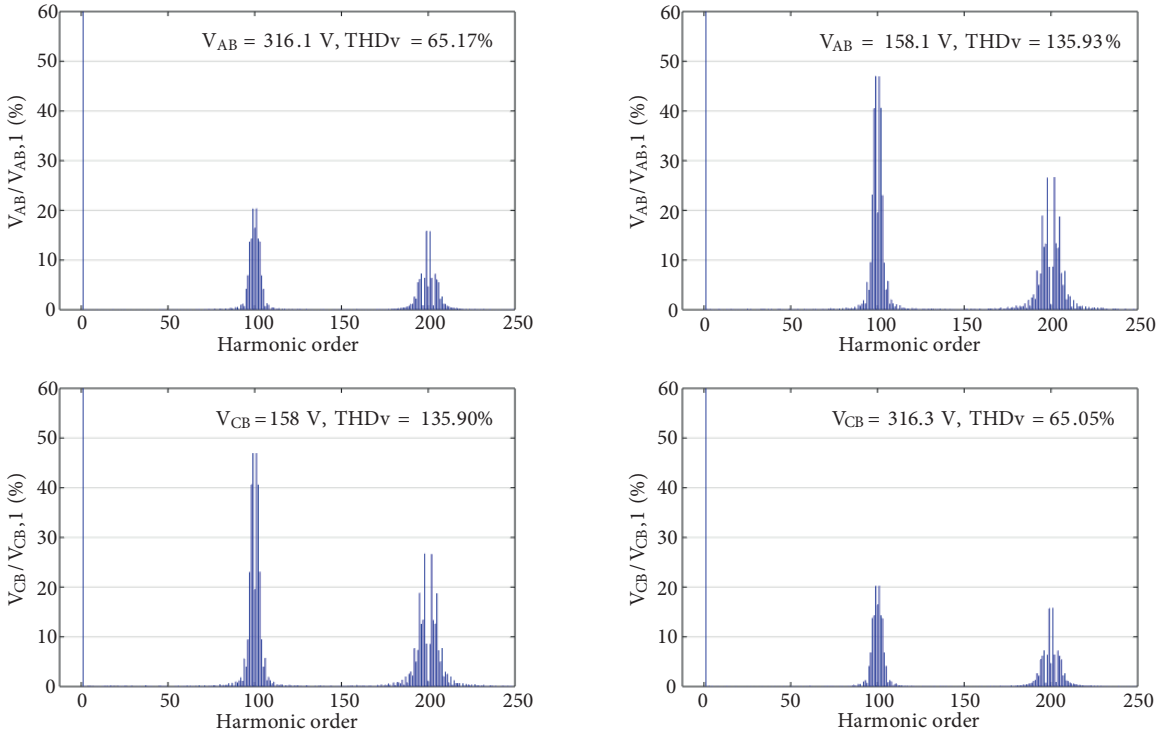

Figure 8. Harmonic spectrum of the discontinuous SVM technique for unbalanced two-phase three-leg inverter: a) $\theta_v = +36.87^\circ$ with DSVM-1, b) $\theta_v = -36.87^\circ$ with DSVM-2.

4.2. Simulation and experimental results of the discontinuous SVM technique for the unbalanced two-phase three-leg inverter controlling asymmetrical two-phase induction motor

The proposed unbalanced SVM technique for the three-leg inverter applied to the asymmetrical two-phase induction motor (TPIM) has been verified by simulation and experimental results. The block diagram and the experimental test bench of the proposed system are shown in Figure 9, responsible for determining the modulating signals and distributing the corresponding generating pulses. The two-phase three-leg inverter operates over the 1/2-hp asymmetrical TPIM with standard V/f control. The DC-link voltage V_{dc} is 500 V, and the switching frequency f_s is 5 kHz. Also, the shift-angle θ_v was set at 30° as the turns ratio of windings is 1.71.

Using the proposed discontinuous SVM technique applied to the asymmetrical TPIM drive system, Figure 10 shows the simulated waveform under the unit step changing from DSVM-1 to DSVM-2 at 0.86 s. Figure 10a shows the simulation results of the discontinuous modulating signals and gating pulses. It can be seen that the gating pulses of the inverter are not switched continuously during the fundamental period. The output voltage and current waveforms at the full load torque are shown in Figure 10b, Figure 10c, and Figure 10d, respectively. It can be seen that output voltages v_{AB}, v_{CB} and currents i_A, i_C with the orthogonal are unbalanced. From the result in Figure 10d, it can be observed that output current i_A leads output current

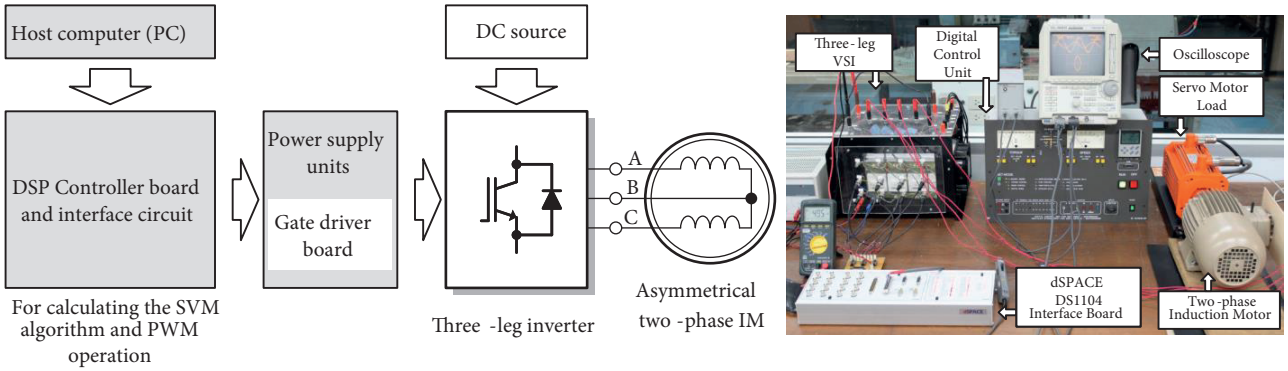

Figure 9. The configuration of a two-phase induction motor drive using the proposed SVM technique.

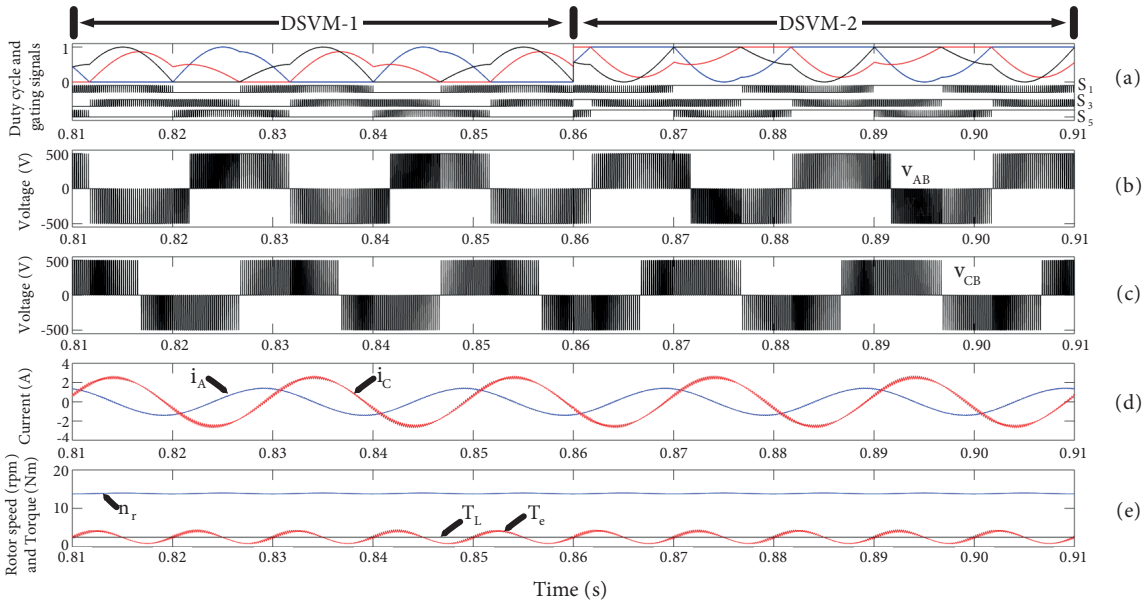

Figure 10. Simulated waveforms of the proposed SVM technique for two-phase three-leg inverter applied to the asymmetrical TPIM drive system: a) duty cycles and gating pulses, b) output voltage v_{AB}, c) output voltage v_{CB}, d) output currents i_A and i_C.

i_C, in which the magnitudes are unequal and the phase difference angle is fixed at 90°. Figure 10e shows the rotor speed and torque of the asymmetrical TPIM with a constant full load torque, 2.5 Nm.

Two dynamic tests of the discontinuous SVM technique for the unbalanced two-phase three-leg inverter drive system are performed in Figure 11. The discontinuous modulating signals and gating pulses when the SVM technique is changing unit step from DSVM-1 to DSVM-2 are shown in Figure 11a. It can be easily seen that the experimental waveforms are the same as the theoretical and simulated results. Figure 11b shows the voltages v_{AB}, v_{CB} and currents i_A, i_C of the drive system. The output voltages are generated unbalanced voltages supplied to the asymmetrical TPIM due to the turns ratio of machine windings. The two-phase output currents are unequal magnitude sinusoidal waveforms where both currents are regulated by 90°. Therefore, the proposed SVM technique can be used in the unbalanced two-phase three-leg inverter for the asymmetrical TPIM drive system.

Figure 12 shows experimental waveform analysis of the output current under no-load, half-load, and full-load torque. It can be seen that the current of the return middle leg in a three-leg inverter is calculated from $i_B = i_A + i_C$, which can be easily seen from Figure 12a. Therefore, the rated current of the power switch in leg-B should be higher. To further the torque pulsation effect of the amplitude unbalanced output currents, the steady-state generated motor torque and load torque responses are shown in Figure 12b. The proposed approach can reduce the generated torque pulsations and noise signals.

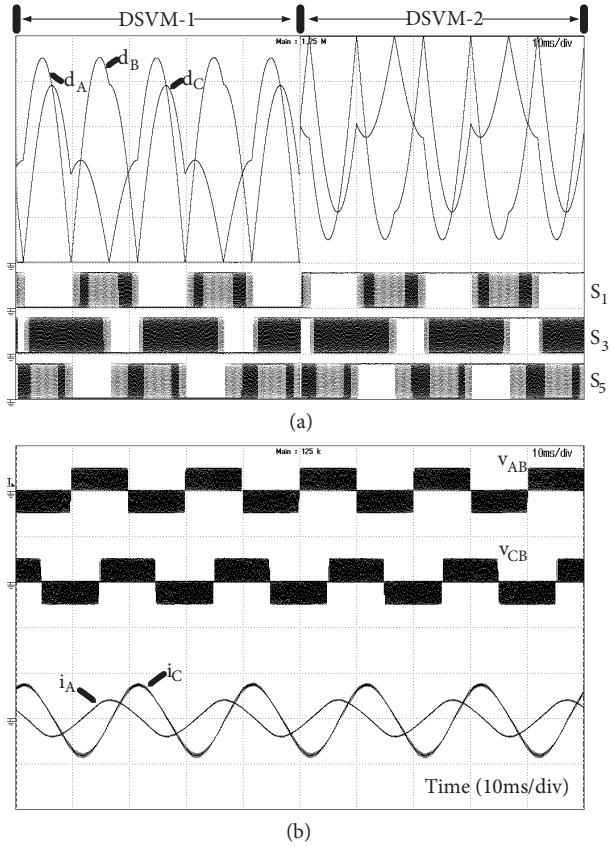

Figure 11. Experimental waveforms of the proposed SVM technique for two-phase three-leg inverter applied to the asymmetrical TPIM drive system: a) duty cycles d_A, d_B, and d_C (2V/div) and gating pulses S_1, S_3, and S_5 (20V/div); b) output voltages, v_{AB} and v_{CB} (1000 V/div) and currents i_A and i_C (2 A/div).

To verify the proposed SVM technique, the results for all switching patterns are shown in Figure 13. In Figure 13a, it is obvious that, under the conventional modulation technique, each switch is turned on and off in two timer switching cycles, i.e. six commutations per switching cycle. Figure 13b shows the negative clamped modulation technique (DSVM-1), while Figure 13c shows the positive clamped modulation technique (DSVM-2). Under the proposed discontinuous modulation techniques, the switching state is commuted four times in each switching cycle. It can be noted that the gating pulses of the proposed technique are not switched continuously in its time period, resulting in a lower number of commutations for one-third of the fundamental period compared to the conventional modulation technique.

By properly setting the amplitude and frequency of the unbalanced two-phase output voltage for the asymmetrical TPIM by using the proposed modulation technique, it can be operated at the intersection point of the torque–speed characteristic curve of the motor as shown in Figure 14a. When the load torque changes, the

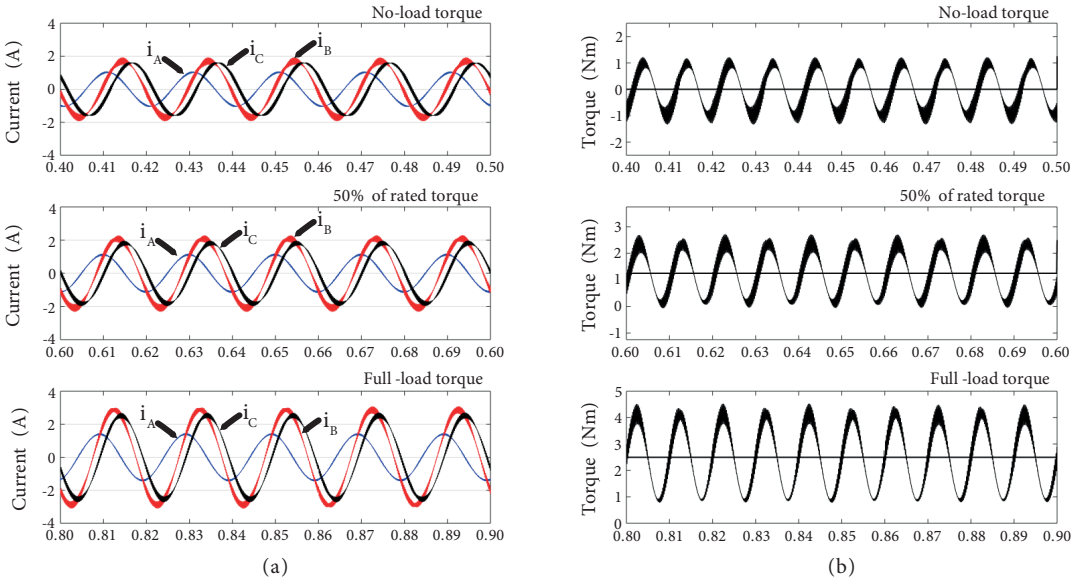

Figure 12. Experimental waveform analysis of the proposed discontinuous SVM technique for unbalanced two-phase three-leg inverter applied to asymmetrical TPIM drive system: a) output currents, b) torque pulsation.

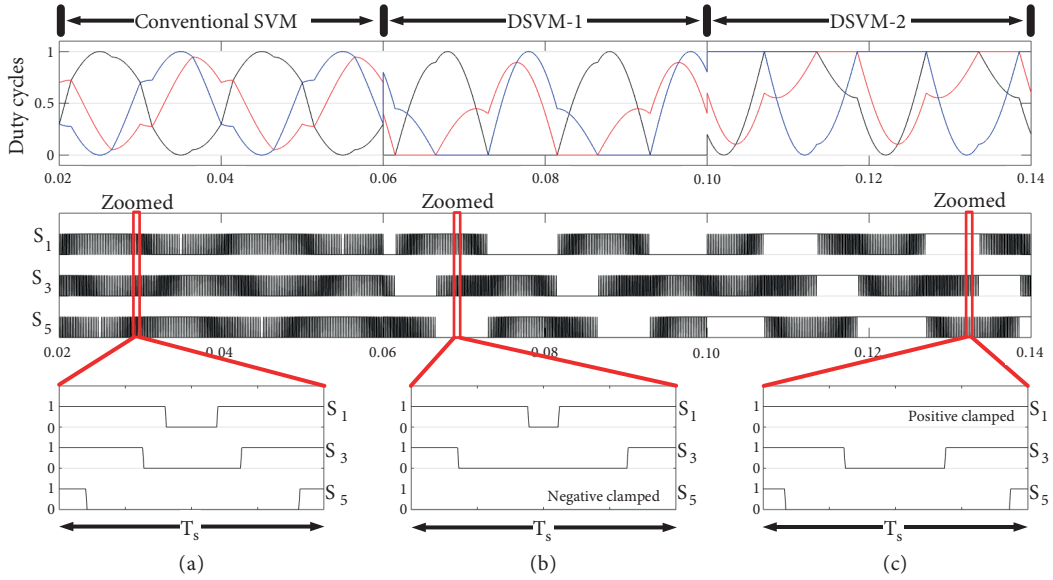

Figure 13. Experimental waveform analysis of switching patterns in time period: a) conventional SVM, b) DSVM-1, and c) DSVM-2.

standard amplitude and frequency control is adjusted such that the motor can operate at another intersection point. Finally, the efficiency of the inverter system is measured using the conventional SVM, DSVM-1, and DSVM-2, where the obtained results are as shown in Figure 14b. This result confirms the merit of having a reduced number of commutations, where higher efficiency can be reached.

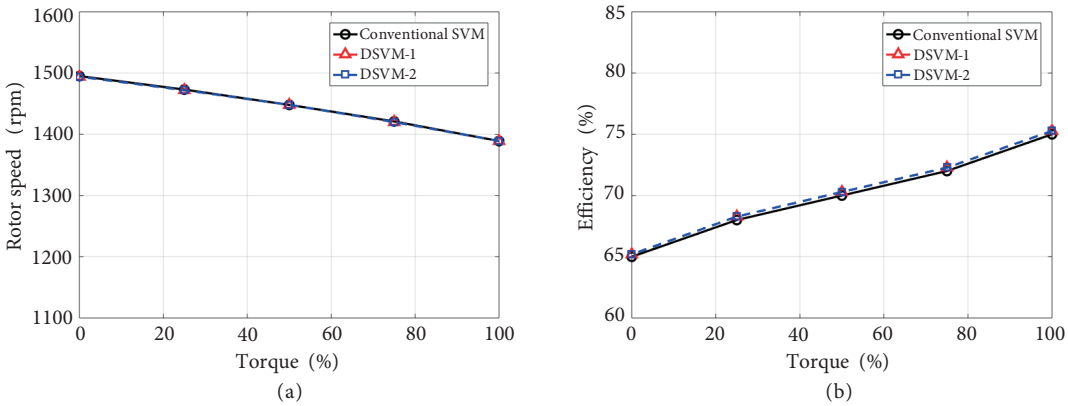

Figure 14. Performance comparison of the proposed discontinuous SVM technique for unbalanced two-phase three-leg inverter applied to asymmetrical TPIM drive system: a) torque-speed characteristics, b) measured efficiency of the proposed inverter system using different modulation techniques at different load torque conditions.

5. Conclusion

A discontinuous SVM technique for unbalanced output voltages based on a two-phase three-leg inverter is presented in this paper. The proposed SVM algorithm is composed step by step, suggesting six variations depending on switching sequence selections. The advantages are simplified modulation technique, reduced switching commutation, and ease for digital control implementation. The feasibility of the proposed modulation technique for the three-leg inverter has been verified by simulation and experimental results. This confirms that the discontinuous SVM technique is able to achieve good performance with quality to the output voltages and currents in dynamic and steady-state conditions. The numbers of commutations compared to the conventional modulation technique are reduced and the voltage leg is distributed more evenly on each power device for about one-third of the cycle. The application of the proposed modulation technique and inverter system is able to achieve good performance for the two-phase load system and the asymmetrical TPIM drive system.

Acknowledgments

This research was supported by the Chiang Mai University Junior Research Fellowship Program, Research Administration Center, Chiang Mai University. The author was also supported by the Office of the Higher Education Commission and the Thailand Research Fund (Grant No. MRG6180135).

References

[1] Holmes H, Lipo T. Pulse Width Modulation for Power Converters: Principles and Practices. Hoboken, NJ, USA: Wiley-IEEE Press, 2003.

[2] Silva E, Santos C, Jacobina C. Pulsewidth modulation strategies: nonsinusoidal carrier-based PWM and space vector modulation techniques. IEEE Ind Electron Mag 2011; 6: 37-45.

[3] Holtz J. Pulsewidth modulation for electronic power conversion. P IEEE 1994; 82: 1194-1214.

[4] Kolar J, Ertl H, Zach F. Influence of the modulation method on the conduction and switching losses of a PWM converter system. IEEE T Ind Appl 1991; 27: 1063-1075.

[5] Abdelhakim A, Davari P, Blaabjerg F, Mattavelli P. Switching loss reduction in the three-phase quasi-Z-source inverters utilizing modified space vector modulation strategies. IEEE T Power Electron 2018; 33: 4045-4060.

[6] Ojo O. The generalized discontinuous PWM scheme for three-phase voltage source inverters. IEEE T Ind Electron 2004; 51: 1280-1289.

[7] Hobraiche J, Patin N, Friedrich G, Vilain J. A direct digital technique implementation of general discontinuous pulse width modulation strategy. IEEE T Ind Electron 2001; 58: 4445-4454.

[8] Gohil G, Maheshwari R, Bede L, Kerekes T, Teodorescu R, Liserre M, Blaabjerg F. Modified discontinuous PWM for size reduction of the circulating current filter in parallel interleaved converters. IEEE T Power Electron 2015; 30: 3457-3470.

[9] Dalessandro L, Round S, Drofenik U, Kolar J. Discontinuous space-vector modulation for three-level PWM rectifiers. IEEE T Power Electron 2008; 23: 530-542.

[10] Asiminoaei L, Rodriguez P, Blaabjerg F. Application of discontinuous PWM modulation in active power filters. IEEE T Power Electron 2008; 23: 1692-1706.

[11] Lakhimsetty S, Surulivel N, Somasekhar V. Improvised SVPWM strategies for enhanced performance for a four-level open-end winding induction motor drive. IEEE T Ind Electron 2017; 64: 2750-2759.

[12] Lin H, Kwon B, Space-vector PWM techniques for a two-phase permanent magnet synchronous motor considering a reduction in switching losses. J Electr Eng Technol 2015; 10: 742-752

[13] Jang DH, Yoon DY. Space-vector PWM technique for two-phase inverter-fed two-phase induction motors. IEEE T Ind Appl 2003; 39: 542-549.

[14] Jabbar M, Khanbadkone A, Yanfeng Z, Space-vector modulation in a two-phase induction motor drive for constant-power operation. IEEE T Ind Electron 2004; 51: 1081-1088.

[15] Jang DH. PWM methods for two-phase inverters. IEEE T Ind Appl Mag 2007; 13: 50-61.

[16] Kinnares V, Charumit C. Modulating functions of space vector PWM for three-leg VSI-fed unbalanced two-phase induction motors. IEEE T Power Electron 2009; 24: 1135-1139.

[17] Charumit C, Kinnares V. Discontinuous SVPWM techniques of three-leg VSI-fed balanced two-phase loads for reduced switching losses and current ripple. IEEE T Power Electron 2015; 30: 2191-2204.

[18] Liaw C, Chiang S. Design and implementation of a single-phase three-wire transformerless battery energy storage system. IEEE T Ind Appl 1994; 41: 540-549.

[19] Tanaka T, Sekiya T, Tanaka H, Okamato M, Hiraki E. Smart charger for electric vehicles with power-quality compensator on single-phase three-wire distribution feeders. IEEE T Ind Appl 2013; 49: 2628-2635.

[20] Kuo Y, Liang T, Chen J. A high-efficiency single-phase three-wire photovoltaic energy conversion system. IEEE T Ind Electron 2003; 50: 116-122.

[21] Kumsuwan Y, Premrudeepreechacharn S, Kinnares V. A carrier-based unbalanced PWM method for four-leg voltage source inverter fed unsymmetrical two-phase induction motor. IEEE T Ind Electron 2013; 60: 2031-2041.